A study on characteristic indexes of railway ballast bed under high-frequency radar

Shilei Wang, Zhan Peng, Guixian Liu, Weile Qiang and Chi Zhang

Infrastructure Inspection Research Institute,
China Academy of Railway Sciences Corporation Limited, Beijing, China

Abstract

Purpose – In this paper, a high-frequency radar test system was used to collect the data of clean ballast bed and fouled ballast bed of ballasted tracks, respectively, for a quantitative evaluation of the condition of railway ballast bed.

Design/methodology/approach – Based on original radar signals, the time–frequency characteristics of radar signals were analyzed, five ballast bed condition characteristic indexes were proposed, including the frequency domain integral area, scanning area, number of intersections with the time axis, number of time-domain inflection points and amplitude envelope obtained by Hilbert transform, and the effectiveness and sensitivity of the indexes were analyzed.

Findings – The thickness of ballast bed tested at the sleep bottom by high-frequency radar is up to 55 cm, which meets the requirements of ballast bed detection. Compared with clean ballast bed, the values of the five indexes of fouled ballast bed are larger, and the five indexes could effectively show the condition of the ballast bed. The computational efficiency of amplitude envelope obtained by Hilbert transform is $140 \, \text{s} \cdot \text{km}^{-1}$, and the computational efficiency of other indexes is $5 \, \text{s} \cdot \text{km}^{-1}$. The amplitude envelopes obtained by Hilbert transform in the subgrade sections and tunnel sections are the most sensitive, followed by scanning area. The number of intersections with the time axis in the bridge sections was the most sensitive, followed by the scanning area. The scanning area can adapt to different substructures such as subgrade, bridges and tunnels, with high comprehensive sensitivity.

Originality/value – The research can provide appropriate characteristic indexes from the high-frequency radar original signal to quantitatively evaluate ballast bed condition under different substructures.

Keywords Ballasted track, Ballast bed, High-frequency radar, Test, Time–frequency characteristics, Characteristic indexes

Paper type Research paper

1. Introduction

Ballast bed is the foundation of ballasted track for conventional railway and high-speed railway with a speed of 200–250 km/h (Ye, Cai, Zhang, Wei, & Yan, 2021). With the increase of service time and the gross traffic tonnage of a line, ballast bed will gradually deteriorate, which undermines its elasticity and drainage performance, and frequent maintenance will be required, even cleaning and overhaul. Many factors contribute to the deterioration of ballast bed, such as the gross traffic tonnage, traffic conditions, ballast quality, subgrade quality,

environmental factors, climatic conditions, etc. (Rohrman & Ho, 2019; Rohrman, Kashani, & Ho, 2020; Xu, Gao, Jing, Cai, & Luo, 2015). According to the current rule of track repair, the ballast bed cleaning cycle mainly depends on the gross traffic tonnage of the line and shall be appropriately adjusted according to the *in situ* boring test results for the percentage of fouling (China State Railway Group Co., Ltd., 2019). A cleaning strategy developed only based on the gross traffic tonnage may lead to overrepair or underrepair of ballast bed. With the percentage of fouling test data, scientific decisions for cleaning can be better made. However, the traditional percentage of fouling tests are mainly made by onsite sampling and laboratory screening method (Qie, Xu, Li, Wang, & Wang, 2020), which is inefficient and will cause certain disturbance to the line, so this method is limited for application. The insufficient boring test point data cannot fully reflect the ballast bed condition of the entire railway network. With the expansion of railway scale and the increasing shortage of ballast resources (Jing, Huang, Chang, & Qiang, 2017; Morata, 2017), it is urgent to develop a rapid detection technology for ballast bed condition at the railway network level (Niu, 2020), so as to scientifically formulate the repair schedule and reasonably allocate resources and control costs.

For the rapid and nondestructive advantages of ground penetrating radar detection and quantitative evaluation of ballast bed, a lot of research and practice on this technology have been carried out abroad in the past 10 years. Silvast, Nurmikolu, and Wiljanen (2010) employed the radar signal frequency domain integration as a characteristic index to indicate ballast bed fouling and established the relationship between the characteristic index and the ballast bed fouling index through *in situ* sampling to realize the classified management of ballast bed condition of railways in Finland. Shangguan, Al-qadi, and Leng (2012) proposed a method for quantifying ballast bed fouling by using the standard deviation of specific series of wavelet signals as a characteristic index. Roberts, Al-qadi, Tutumluer, and Kathage (2006) discovered the void scattering of high-frequency radar waves in the clean ballast bed, and, together with Al-qadi, Xie, and Roberts (2008), proposed an analysis method by adding Hilbert transform and smoothing processing on the basis of conventional radar image processing steps through analysis and verification of radar data of a 614 km line in operation and developed a piece of software to display spectra of ballast bed fouling in layers based on the scattering amplitude envelopes. Zetica Rail, a United Kingdom company, developed a ballast bed testing system based on high-frequency radar (Zhang, Eriksen, & Gascoyne, 2010) and established the ballast layer geometry index and ballast fouling index. The latter is calculated according to the scattering signal characteristics and calibrated according to *in situ* sampling and laboratory screening results. The Shuohuang Railway Company of China introduced this system in 2015 to guide the ballast bed cleaning of coal transportation lines (Qin, 2017). The United States Transportation Technology Center Co., Ltd. successively carried out comparative tests on the ballast bed condition test performance of six different radar systems on its heavy load loop and other railways in operation, and the test results showed that low-frequency radar (400 MHz) can be used to identify the layers of ballast bed and subgrade bed, and high-frequency radar (2 GHz) can realize fine feedback of the development of ballast bed fouling. Subsequently, studies such as high-frequency ground penetrating radar carrier and environmental adaptability tests, high-frequency ground penetrating radar technology evaluation and implementation were carried out successively, and the system was integrated into the DOTX-220 track inspection vehicle of the Federal Railroad Administration in 2020 for a time-space synchronous inspection of track geometry and ballast bed condition (Federal Railroad Administration, 2017a, b, 2020). It can be seen that high-frequency radar technology is mainly used outside of China to detect fouling, which is a key indicator of ballast bed condition for cleaning planning. At present, there are few studies on this technology in China, so it is necessary to study the feasibility of this technology and the key analysis method of radar signals.

In this paper, a high-frequency radar test system was used to collect the data of clean and fouled ballast bed of a ballasted track line in operation, respectively, and analyze the time–frequency characteristics of radar signals, and five ballast bed condition characteristic indexes were designed based on the original radar signals, and the effectiveness and sensitivity of the indexes were studied.

2. High-frequency radar test

2.1 Test principle and equipment

The schematic diagram of radar detection technology for ballast bed is shown in Figure 1 (Tosti, Ciampoli, Calvi, Alani, & Benedetto, 2018). The transmitting antenna transmits electromagnetic waves into the ballast bed. When encountering a boundary layer or area with different dielectric properties, the electromagnetic waves will be reflected and scattered. The receiving antenna will then record the time and amplitude of the return waves to form a single-channel waveform, and a two-dimensional (2D) radar image composed of multiple-channel waveforms can be generated with samples taken at a specified longitudinal interval along the line. Through the analysis of single-channel wave signals and 2D radar images, the distribution characteristics in terms of ballast thickness, ballast bed fouling, poor drainage and other aspects concerned with track maintenance and repair can be obtained.

The 2 GHz center frequency air-coupled antenna and supporting main control equipment of Exploration Geophysics, Inc. were used for the test. The acquisition was carried out under distance trigger mode, with a time window of 25 ns, 512 sampling points set, a trace interval of 5 cm and no gain adjustment during acquisition. The acquisition unit was mounted on the manually pushed coaxial rotating insulated wheel metal frame trolley to collect the ballast shoulder ballast bed condition data. The test antenna was set according to the vehicle clearance requirements at the upper part of the concrete sleeper end, with the polarization direction consistent with the line direction, and the bottom surface of the antenna was about 400 mm from the ballast surface. The test speed was about $3 \, \text{km} \cdot \text{h}^{-1}$. The composition of the test system is shown in Figure 2.

2.2 Test section

The condition test of railway ballast bed based on high-frequency radar was carried out in the section $K36 + 600 - K38 + 700$ of a Class I railway and the section $K188 + 500 - K191 + 500$ of a Class I railway in North China.
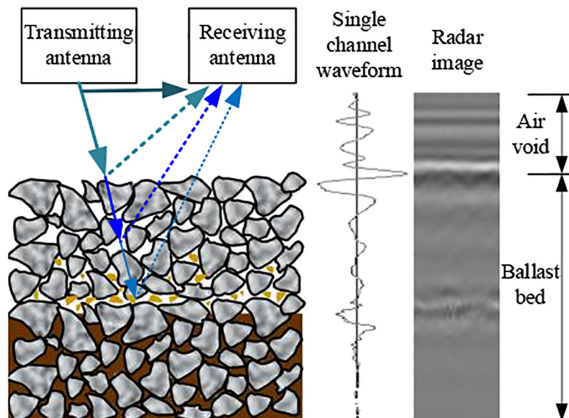

Figure 1.
Schematic diagram of radar detection technology for ballast bed

Filled subgrade is adopted in the section K36 + 600 − K38 + 700 of the up track of the subject Class I railway, Type II concrete sleepers are laid on the track with a spacing of 60 cm and the annual gross traffic tonnage of the line is about 83 Mt. The test section K36 + 600 − K37 + 000 was cleaned by a large full-section ballast cleaning machine in 2018, and section K37 + 000 − K38 + 700 was cleaned in 2010. The test was carried out in early September 2020. No rainfall was observed one week before the test, and the inside of the ballast bed was basically dry. In 2010, the ballast shoulder in some cleaning sections was seriously fouled, and the agglomeration phenomenon of black fine-grained coal was found when the top ballast particles were removed. The layout of the test sections and the condition of the ballast bed at typical positions are shown in Figure 3.

Test section K188 + 500 − K191 + 500 of the subject Class II railway includes two tunnels, which are 1,266 m and 137 m long, respectively, and two simply-supported prestressed concrete T-beam bridges, which are 100 m and 175 m long, respectively. Type II concrete sleepers are used in the subgrade section of the test section, and Type III concrete sleepers are used in the tunnel and bridge sections, with a spacing of 60 cm. The annual gross freight tonnage of the line, mainly coal, is about 37 Mt. The tunnel sections in the test section were manually cleaned in 2019, and the subgrade and bridge sections had not been cleaned for 15 years. The test was carried out at the end of September 2020, and no rainfall was observed 1 week before the test. Upon patrol inspection, it was found that the inside of the ballast bed in the test section was basically dry, and there was intermittent mud pumping at the mid-track and the sleeper end in the sections that had not been cleaned for years. The layout of the test sections and the condition of the ballast bed at typical positions are shown in Figure 4.
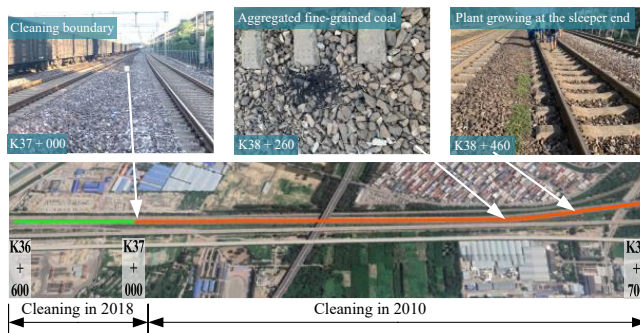
3. Test results

3.1 Relative dielectric constant

The relative dielectric constant ε_r is a parameter used to characterize the dielectric properties of the medium and to calculate the propagation velocity of electromagnetic waves and can be calculated by the following equation:

$$\varepsilon_r = \left(\frac{0.3t}{2d}\right)^2 \tag{1}$$

where t is the two-way travel time of radar wave between two interfaces (in ns); d is the distance between two interfaces (in m).

The results show that the relative dielectric constant of dry ballast bed generally ranges from 4 to 7, a low value should be taken for clean ballast bed and a high value for fouled ballast bed (Barrett, Day, Gascoyne, & Eriksen, 2019).

A test borehole was set at K191 + 073 of the subject Class II railway. The radar image of the tested ballast bed and the test borehole condition are shown in Figure 5. The boring test revealed that the distance between the ballast surface and the ballast bottom is 53 cm, the thickness of the ballast at the sleeper bottom is 30 cm and the sand bedding is set under the ballast. The reflected radar signal at the bottom of the ballast bed in the tested section is clear, and the two-way travel time of the reflected signal is about 8.7 ns. The relative dielectric constant of the ballast bed calculated by Equation (1) is around 6. A high relative dielectric constant indicates that the fouling degree of the ballast bed is high, since it is related to the accumulation of fine-grained coal in ballast voids as revealed by the boring test.
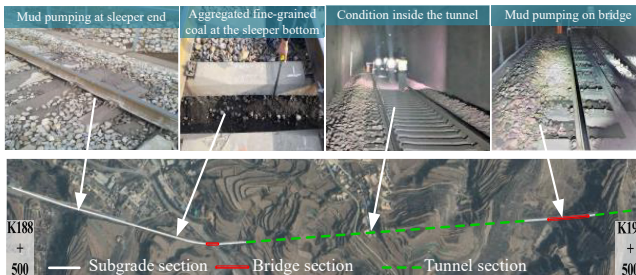

Figure 4.
Layout of test sections
of a Class II railway
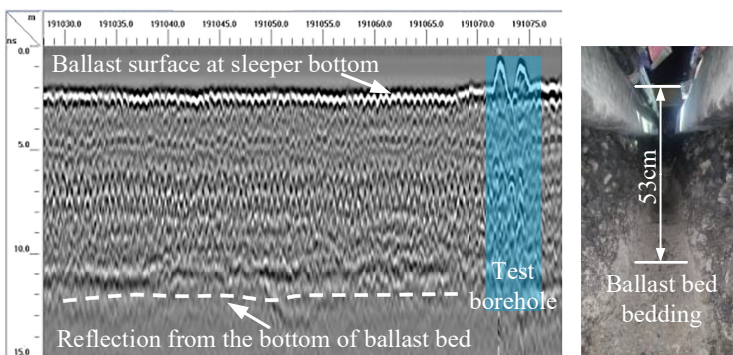and ballast bed
condition at typical
positions

Figure 5.
Radar image of tested
ballast bed section and
test borehole condition

3.2 Time–frequency characteristics of radar signals

Figure 6 shows the time-domain waveforms of radar signals under different ballast bed conditions of the subject Class I railway. Figure 6(a) shows the time-domain waveform of radar signals of clean ballast bed at K36 + 800 for the ballast cleaning in 2018, and Figure 6(b) shows the time-domain waveform of radar signals of fouled ballast bed at K38 + 260 for the ballast cleaning in 2010.

It can be seen from Figure 6 that the two-way travel time within the effective signal range inside the clean ballast bed is about 12.7 ns, and the dielectric constant is conservatively taken as 6. According to Equation (1), the effective detection thickness is about 77 cm down from the ballast surface. After deducting the sleeper height, the effective detection depth of the ballast bed at the sleeper bottom is about 55 cm, which can meet the detection requirements for ballast bed. By comparing Figure 6(a) and (b), it can be found that the high-frequency signal response of fouled ballast bed is more evident than that of clean ballast bed.

By further converting the single-channel waveforms under the two types of ballast bed condition by fast Fourier transform, the radar signal spectra under the two types of ballast bed condition were obtained, as shown in Figure 7.

It can be seen from Figure 7 that the energy amplitude of the frequency component greater than 2 GHz of the radar signal of the clean ballast bed is small, the energy amplitude of the
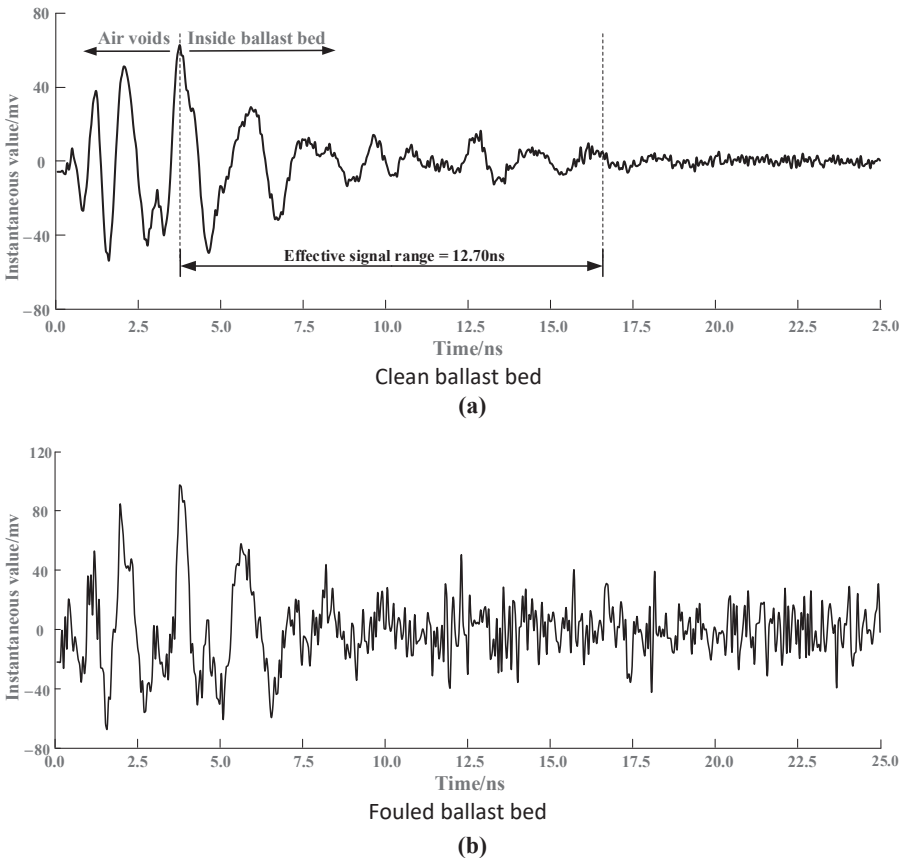

Figure 6.
Time-domain waveforms of radar signals under different ballast bed conditions of Class I railway

fouled ballast bed is higher than that of the clean ballast bed at most frequencies and the fouled ballast bed has a larger envelope area than that of the clean ballast bed.

4. A study on characteristic indexes of ballast bed condition
4.1 Characteristic indexes and extraction methods
From the above analysis, it can be seen that the electromagnetic signal time–frequency characteristics of clean ballast bed and fouled ballast bed are significantly different, which provides the basis for analyzing the condition of ballast bed. In order to further quantify the ballast bed condition, characteristic indexes of ballast bed condition based on radar electromagnetic signals are required.

The laboratory model test results show that there is a potential strong correlation between the frequency domain integral area S_{fRa}, the scanning area S_{tAb}, the number of intersections with the time axis $C_{ross\text{-}Num}$, the number of time-domain inflection points $I_{nflec\text{-}Num}$ and the amplitude envelope obtained by Hilbert transform H_{ht} and the ballast bed condition (Al-qadi *et al.*, 2008; De Bold, O'connor, Morrissey, & Forde, 2015; Silvast *et al.*, 2010). The construction idea of the indexes is shown in Figure 8.

The frequency domain integral area is obtained by integrating the ballast bed signal spectrum converted by the Fourier transform along the frequency axis, as the shadowed envelope in Figure 8(a). The scanning area is obtained by integrating the absolute value of the instantaneous value of the time-domain signal inside the ballast bed along the time axis, as the shadowed envelope in Figure 8(b). The number of intersections with the time axis refers to the number of intersections between the time-domain signal inside the ballast bed and the time axis, as circled in Figure 8(c). The number of time-domain inflection points refers to the number of turning points of the time-domain signal inside the ballast bed where the signal makes an upward/downward turn, as marked by X-crossing in Figure 8(d). The amplitude envelope obtained by Hilbert transform is the area of the amplitude envelope obtained by integrating the time-domain signal inside the ballast bed processed by Hilbert transform along the time axis, as shown by the shadowed envelope in Figure 8(e).

Since it is impossible to distinguish air voids from the inside of ballast bed based on the horizontal axis of the frequency domain, the integral area of the frequency domain is computed based on the signal information as a whole, and the other four indexes are only extracted from the signal information of the ballast bed. It should be noted that, unlike the conventional ground penetrating radar image interpretation method, the data used in this paper are all from the original radar signals without background subtraction and gain
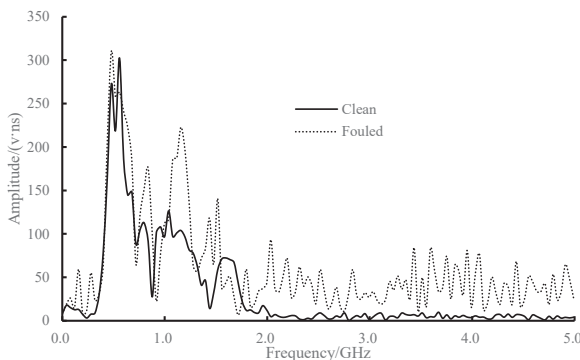

Figure 7.
Radar signal
spectrums under
different ballast bed
condition

Frequency domain S_{fRa}

(a)

Scanning area S_{tAb}

(b)

Number of intersections with the time axis $C_{ross-Num}$

(c)

Number of time-domain inflection points $I_{nflec-Num}$

(d)

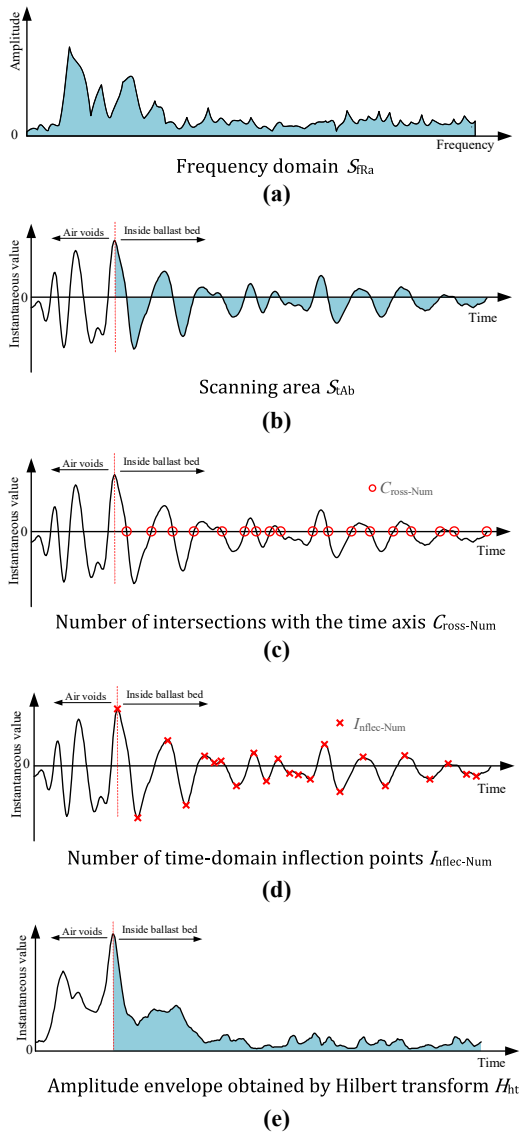Amplitude envelope obtained by Hilbert transform H_{ht}

(e)

Figure 8.
Schematic diagram for construction of characteristic indexes of ballast bed condition

adjustment, so as to ensure a standard construction method of characteristic indexes and facilitate the promotion of the method.

Extraction of characteristic indexes mainly consists of four steps: test data array extraction, data analysis range determination, characteristic value sequence establishment and characteristic value line direction smoothing. Taking the scanning area as an example, the extraction steps are shown in Figure 9. The data range is determined in two steps: determining the serial number of each sampling point corresponding to ballast bed surface reflection and filtering out signals of air voids.
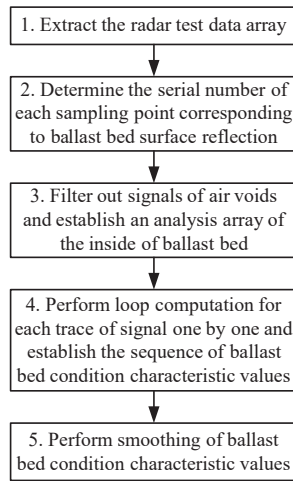
1. Extract the radar test data array
2. Determine the serial number of each sampling point corresponding to ballast bed surface reflection
3. Filter out signals of air voids and establish an analysis array of the inside of ballast bed
4. Perform loop computation for each trace of signal one by one and establish the sequence of ballast bed condition characteristic values
5. Perform smoothing of ballast bed condition characteristic values

Figure 9.
Extraction steps of
scanning area

The cyclic solution flow to establish the sequence of characteristic values of ballast bed condition is shown in Figure 10. In the figure, $\boldsymbol{P}$ is the ballast bed radar signal data array, which consists of l row(s) and m column(s) of data, each column of data corresponds to a single channel signal, l is the number of data sampling points obtained after the filtration of air voids of the single channel signal and m is the channel number of data acquisition for the
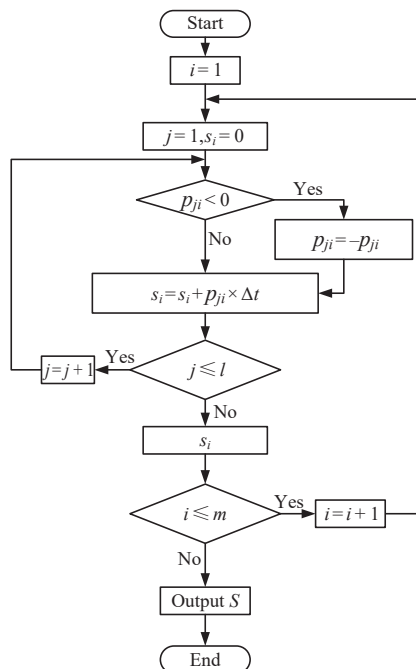
Start

$i=1$

$j=1, s_i=0$

$p_{ji} < 0$ — Yes → $p_{ji} = -p_{ji}$

No

$s_i = s_i + p_{ji} \times \Delta t$

$j \leq l$ — Yes → $j = j + 1$

No

s_i

$i \leq m$ — Yes → $i = i + 1$

No

Output S

End

Figure 10.
Computation loop of
scanning area
characteristic value
sequence

test line; Δt is the time difference between adjacent rows; i and j are the variables in cyclic computation, and p_{ij} indicates the value of the element in row i and column j of array $\boldsymbol{P}$; $\boldsymbol{S}$ is the sequence of characteristic index value to be solved, and S_i indicates the element value i to be solved in the sequence.

*4.2 Effectiveness and sensitivity of indexes*
Combined with the field investigation and track maintenance records, the radar test data of 24 m each of the clean ballast bed of section $K36 + 828 - K36 + 852$ and the fouled ballast bed of section $K38 + 248 - K38 + 272$ of the subject Class I railway were selected as samples to test the effectiveness and sensitivity of the five characteristic indexes for ballast bed condition described above. In order to facilitate comparative analyses, the calculation results of each index were subject to max normalization. The calculation results are shown in Figure 11.

It can be seen from Figure 11 that there are high-frequency oscillations in all five index values, and all peak values occur in the concrete sleeper area and all valley values occur in the ballast bed area between sleepers, which is related to the small radar signal sampling tracks (5 cm) and the large difference in radar signals of ballast bed between sleepers. In order to suppress the oscillation phenomenon, the line is divided into units, each of which was 2.4 m long, corresponding to the total length of four sleepers along the longitudinal direction for each index, and the index values in the units are averaged. The processed results are indicated by "means" in Figure 11. Through analyses of the means of characteristic indexes in Figure 11, it can be found that compared with the clean ballast bed, the means of the five indexes of the fouled ballast bed are larger, indicating that the five indexes can characterize the differences in ballast bed condition within the range of sample data.

The sensitivity of each index is analyzed by the max–min ratio of the means of each index extracted from the sample data. Among the five characteristic indexes, the max–min ratio of the amplitude envelope obtained by Hilbert transform is the largest, which is 2.4, indicating that this index is the most sensitive. The max–min ratios corresponding to the scanning area and the number of intersections with the time axis are 1.7 and 1.5, respectively, indicating medium sensitivity. The sensitivity of the frequency domain integral area and the number of time-domain inflection points are the lowest, in which the max–min ratios are 1.3 and 1.2, respectively. Upon assessment of the calculation efficiency of the five characteristic indexes, it is found that the amplitude envelope obtained by Hilbert transform involves empirical modal decomposition, so its calculation efficiency is relatively low. It takes 140 s to calculate data of 1 km, while it only takes 5 s to calculate data for other indexes, that is, the calculation efficiency of the amplitude envelope obtained by Hilbert transform is $140 \text{ s} \cdot \text{km}^{-1}$, and the calculation efficiency of other indexes is $5 \text{ s} \cdot \text{km}^{-1}$.

5. Comparison of different characterization methods for ballast bed condition
In order to analyze the effectiveness of the indexes designed in this paper for characterization of ballast bed condition of lines in operation, the distribution of the three relatively sensitive index values, including amplitude envelope obtained by Hilbert transform, scanning area and intersections with the time axis of the test sections, was calculated in the sections of the subject Class I and Class II railways, respectively. For the convenience of comparison, each index value was subject to max normalization across the test section. Meanwhile, in order to assess the differences between the characterization method for ballast bed condition introduced in this paper with those applied abroad, the method described in the reference (Al-qadi *et al.*, 2008) was used to characterize the ballast bed condition by adding Hilbert
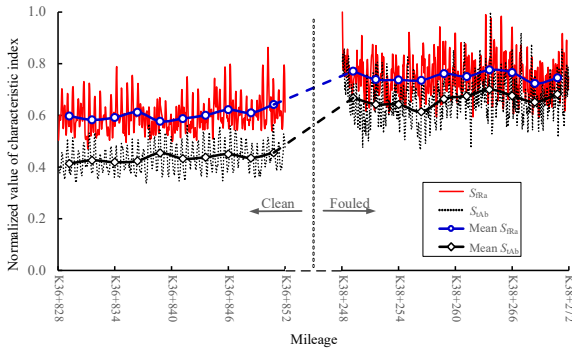
Signal time-domain and frequency-domain areas

(a)
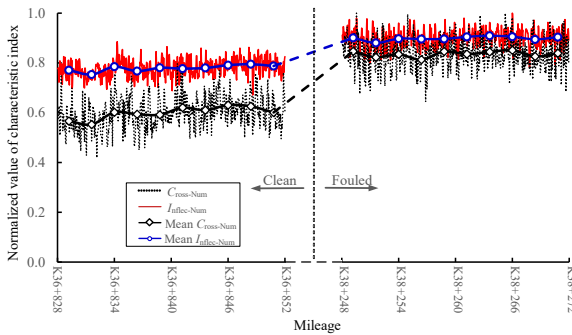
Numbers of intersections with the time axis and inflection
points

(b)
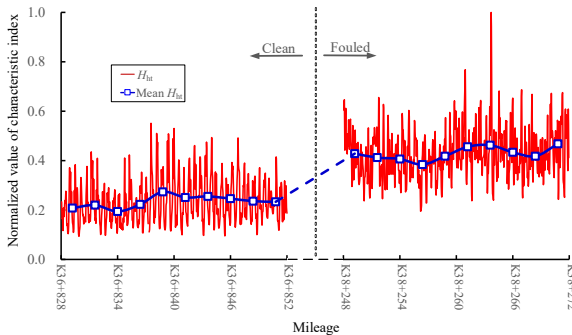
Amplitude envelope obtained by Hilbert transform

(c)

transform to the conventional radar image processing steps to draw the scattering amplitude envelope. The extraction steps for scattering amplitude envelope are shown in Figure 12.

Figure 13 shows the conventional radar image processing results, the scattering amplitude results obtained by Hilbert transform and the distribution of three index values

designed in this paper in the 2,000 m test section (K36 + 600 − K38 + 600) of the subject Class I railway. It can be seen from Figure 13 that the conventional radar signal processing method based on background subtraction and gain adjustment is difficult to visually show the condition of ballast bed, while the readability of the scattering amplitude envelope obtained by Hilbert transform is significantly improved (the envelope amplitude marked in green is the lowest, and the envelope amplitude marked in black is the highest). The envelope amplitude of the cleaning section in 2018 is at a low level, and the envelope amplitude of the cleaning section in 2010 is significantly larger, especially the section after K38 + 000. The section with the highest energy is section K38 + 100 − K38 + 500. Upon ground check, this section is located in a curve with a radius of 2,500 m that is mostly subjected to pulverized coal leakage from trains. The three index values designed in this paper are highly consistent with the scattering amplitude envelope results calculated based on the reference (Al-qadi *et al.*, 2008) along the linear length of the line, and the method presented in this paper can also quantify ballast bed conditions.

Figure 14 shows the analysis results of the 3,000 m test section (K188 + 500 − K191 + 500) of the subject Class II railway. It can be seen from Figure 14 that the three index values of the subgrade section are relatively high and basically consistent with the calculation results based on the method in the reference (Al-qadi *et al.*, 2008). This is related to the fact that no cleaning has been carried out for the line in the past 15 years. The three index values of the tunnel section are low, which is related to the fact that manual cleaning was carried out for the tunnel section in the past two years. Taking the 175 m test section (K191 + 094 − K191 + 269) as an example of bridge sections, the section has not been cleaned for a long time and suffers from severe mud pumping, and the high amplitudes are expected for the indexes. By comparing the calculation results of the three indexes, i.e. the scanning area, the number of intersections with the time axis and the amplitude envelope obtained by Hilbert transform, it is found that the means of the scanning area and the number of intersections with the time axis are 1.5 times and 2.3 times the means of the amplitude envelope calculation results obtained by Hilbert transform, respectively. It shows that the number of intersections with the time axis in the bridge section is the most sensitive, followed by the scanning area, and the amplitude envelope index obtained by Hilbert transform extracted based on the original signals has limitations in the bridge section.

In conclusion, the three characteristic indexes designed in this paper can effectively reflect changes in the condition of ballast bed in subgrade sections and tunnel sections in different years from the last cleaning, of which the amplitude envelope obtained by Hilbert transform is the most sensitive, followed by the scanning area; in bridge sections, the scanning area and the number of intersections with the time axis are more sensitive than the amplitude envelope obtained by Hilbert transform; among the three indexes, the scanning area can adapt to different substructures such as subgrade, bridges and tunnels, and has high comprehensive sensitivity.

6. Conclusions

(1) The effective detection depth of the high-frequency radar test system is about 77 cm and can reach 55 cm at the sleeper bottom for clean ballast bed, which can meet the detection requirements for ballast bed.
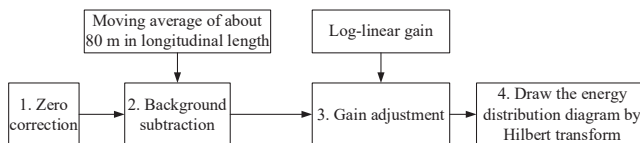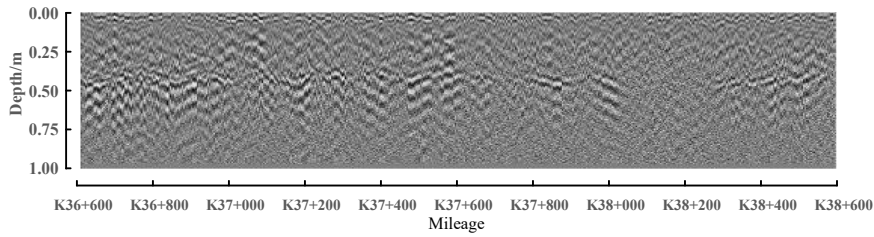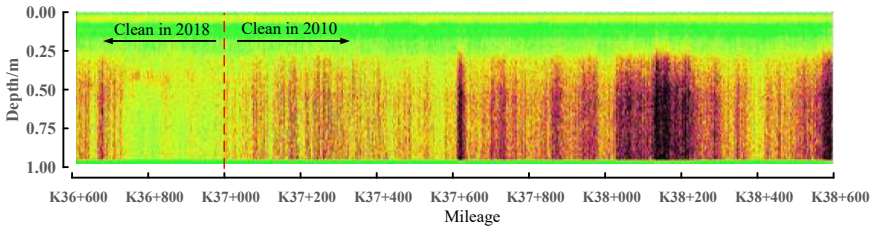
Figure 12.
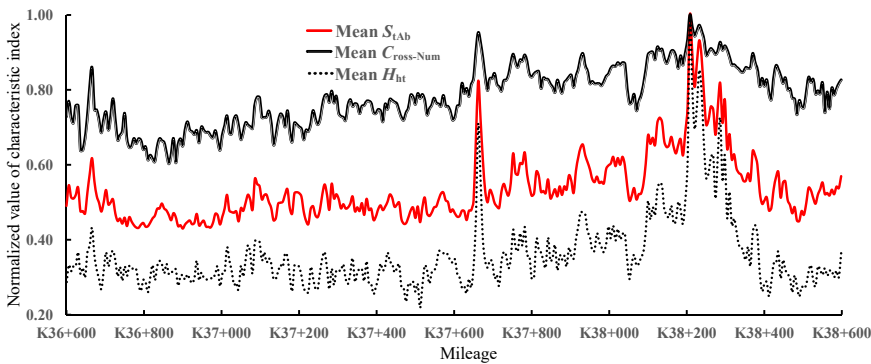Extraction steps for scattering amplitude envelope

Traditional method

(a)

Method in reference(Al-qadi *et al.,* 2008)

(b)

Method in this paper

(c)

(2) Compared with clean ballast bed, the frequency domain integral area, the scanning area, the number of intersections with the time axis, the number of time-domain inflection points and the amplitude envelope obtained by Hilbert transform of fouled ballast bed are all larger, indicating that the five indexes can effectively characterize the ballast bed condition.

(3) The calculation efficiency of amplitude envelope obtained by Hilbert transform is relatively low, which is $140\,\mathrm{s\cdot km^{-1}}$; the calculation efficiency of other indexes is high, which is $5\,\mathrm{s\cdot km^{-1}}$.

Method in Reference (Al-qadi *et al.*, 2008)
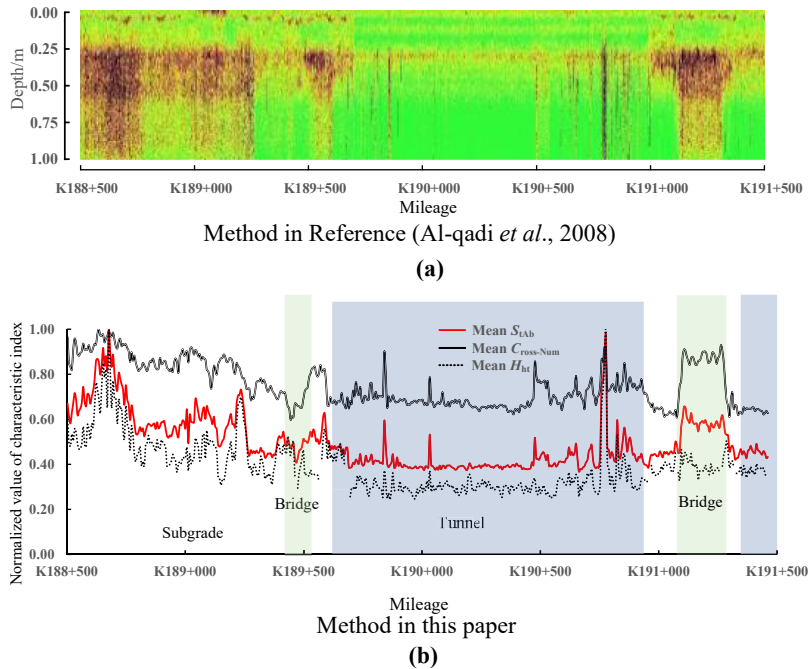
(a)

Method in this paper

(b)

Figure 14.
Comparison of
effectiveness of
different
characterization
methods for ballast bed
condition in test ection
of Class II railway

(4) In subgrade and tunnel sections, the amplitude envelope obtained by Hilbert
transform is most sensitive to the ballast bed condition, followed by the scanning
area. In bridge sections, the scanning area and the number of intersections with time
axis are more sensitive than the amplitude envelope obtained by Hilbert transform.
The scanning area can adapt to different substructures such as subgrade, bridges
and tunnels, with high comprehensive sensitivity.

(5) The characteristic indexes for ballast bed condition designed in this paper are all
derived from the original signal characteristics, without background subtraction,
gain adjustment and other processing, and are suitable for different substructures.
These indexes can provide a benchmark for rapid detection and quantitative
evaluation of ballast bed condition.

References

Al-qadi, I. L., Xie, W., & Roberts, R. (2008). Scattering analysis of ground-penetrating radar data to
quantify Railroad ballast contamination. *NDT & E International*, *41*(6), 441–447.

Barrett, B. E., Day, H., Gascoyne, J., & Eriksen, A. (2019). Understanding the capabilities of GPR for
the measurement of ballast fouling conditions. *Journal of Applied Geophysics*, *169*, 183–198.

China State Railway Group Co., Ltd (2019). *TG-GW 102—2019 Rules for repair of general speed
railway lines*. Beijing: China Railway Publishing House (in Chinese).

De Bold, R., O'connor, G., Morrissey, J. P., & Forde, M. C. (2015). Benchmarking large scale GPR
experiments on railway ballast. *Construction and Building Materials*, *92*, 31–42.

Federal Railroad Administration (2017a). *Ground penetrating radar technology evaluation on the high
tonnage loop: Phase 1*. Technical Report No DOT/FRA/ORD-17/18 (pp. 22–38). Washington, DC:
US Department of Transportation.

Federal Railroad Administration (2017b). *Ground penetrating radar technology evaluation on the high tonnage loop: Phase 2*. Technical Report No DOT/FRA/ORD-17/19 (pp. 66–88). Washington, DC: US Department of Transportation.

Federal Railroad Administration (2020). *Ground penetrating radar (GPR) technology evaluation and implementation*. Report No. DOT/FRA/ORD-20/18 (pp. 102–124). Washington, DC: US Department of Transportation.

Jing, G., Huang, H., Chang, J., & Qiang, W. (2017). Analysis of mechanical characteristics of degradation railway ballast by direct shear test. *Journal of Southwest Jiaotong University*, *52*(6), 1055–1060 (in Chinese).

Morata, M. (2017). Recycled aggregates with enhanced performance for railways track bed and form layers. *Journal of Sustainable Metallurgy*, *3*(2), 322–335.

Niu, D. (2020). Technology and development of railway infrastructure lifetime inspection. *Railway Engineering*, *60*(4), 5–8, 16 (in Chinese).

Qie, L., Xu, Y., Li, M., Wang, H., & Wang, Z. (2020). Evaluation standard of ballast fouling based on permeability. *China Railway Science*, *41*(2), 18–23 (in Chinese).

Qin, H. (2017). Exploration on application of ground penetrating radar to guide ballast cleaning. *Railway Engineering*, *57*(11), 130–133 (in Chinese).

Roberts, R., Al-qadi, I. L., Tutumluer, E., & Kathage, A. (2006). Advances in Railroad ballast evaluation using 2 GHz horn antenna. In *Proceedings of the 11th International Conference on Ground Penetrating Radar* (pp. 889–998), Columbus Ohio, USA. IEEE.

Rohrman, A. K., & Ho, C. L. (2019). Effects of fouling containing plastic fines on abraded ballast strength and deformation properties. *Transportation Geotechnics*, *21*, 100278.

Rohrman, A. K., Kashani, H. F., & Ho, C. L. (2020). Effects of natural abrasion on Railroad ballast strength and deformation properties. *Construction and Building Materials*, *247*, 118315.

Shangguan, P., Al-qadi, I. L., & Leng, Z. (2012). Development of wavelet technique to interpret ground-penetrating radar data for quantifying Railroad ballast conditions. *Transportation Research Record: Journal of the Transportation Research Board*, *2289*(1), 95–102.

Silvast, M., Nurmikolu, A., & Wiljanen, B. (2010). An inspection of railway ballast quality using ground penetrating radar in Finland. *Proceedings of the Institution of Mechanical Engineers, Part F: Journal of Rail and Rapid Transit*, *224*(5), 345–351.

Tosti, F., Ciampoli, L. B., Calvi, A., Alani, A. M., & Benedetto, A. (2018). An investigation into the railway ballast dielectric properties using different GPR antennas and frequency systems. *NDT & E International*, *93*, 131–140.

Xu, Y., Gao, L., Jing, G., Cai, X., & Luo, Q. (2015). Shear behavior analysis of fouled Railroad ballast by DEM and its evaluation index. *Engineering Mechanics*, *32*(8), 96–102 (in Chinese).

Ye, Y., Cai, D., Zhang, Q., Wei, S., & Yan, H. (2021). Current status and development trend of design method for high speed railway subgrade bed structure. *China Railway Science*, *42*(3), 1–12 (in Chinese).

Zhang, Q., Eriksen, A., & Gascoyne, J. (2010). Rail radar—a fast maturing tool for monitoring trackbed. In *Proceedings of the XIII International Conference on Ground Penetrating Radar, Lecce, Italy* (pp. 95–99). IEEE.

Corresponding author
Shilei Wang can be contacted at: thilei@qq.com